Adaptive Spatiotemporal Filtering for Coronary Ultrafast Doppler Angiography

David Maresca, Mafalda Correia, Mickael Tanter, Bijan Ghaleh, Mathieu Pernot

Adaptive Spatiotemporal Filtering for Coronary Ultrafast Doppler Angiography

David Maresca, Mafalda Correia, Mickael Tanter, Bijan Ghaleh, and Mathieu Pernot

***Abstract*— The heart's supply of oxygen and nutrients relies on the coronary vasculature, which branches from millimeter-sized arteries down to micrometer-sized capillaries. To date, imaging technologies can only detect large epicardial coronary vessels, whereas the intramural coronary vasculature remains invisible due to cardiac motion. We recently introduced coronary ultrafast Doppler angiography, a noninvasive vascular imaging technology based on ultrafast ultrasound that enables the visualization of epicardial and intramural coronary vasculature in humans. In this letter we describe, using an open-chest swine data set, the adaptive spatiotemporal filtering method that was developed for the detection of slow blood flows embedded in rapid myocardial motion.**

***Index Terms*— Biomedical imaging, cardiology, Doppler, ultrasonic imaging.**

I. Introduction

THE coronary artery vasculature can be anatomically divided into three compartments: epicardial vessels running along the heart surface (diameters $> 500\ \mu$m), prearterioles that penetrate the myocardium from the epicardium to the endocardium ($500\ \mu\text{m} >$ diameters $> 100\ \mu$m), and the coronary microvasculature (diameters $< 100\ \mu$m) [1].

Existing angiography techniques (X-ray, CT-scans, and MRI) are only capable of imaging epicardial coronary vessels in humans [2], leading cardiology practice to concentrate on focal macroscopic coronary artery disease.

Over the past few years, the sensitivity of Doppler echocardiography has been redefined in the advent of ultrafast ultrasound imaging [3]. Osmanski *et al.* [4] presented a first sparse detection of intramural coronary blood flow detection in open-chest sheep experiments using directional ultrafast power Doppler. In 2014, we showed that ultrafast power Doppler could resolve left ventricle hemodynamics at the millisecond time scale [5]. Here, we report the sliding window, adaptive spatiotemporal filtering strategy that enabled coronary ultrafast Doppler angiography (CUDA) [6] in combination with kilohertz framerate imaging of the heart. The major challenge solved by our signal processing approach consists in detecting low coronary blood flows embedded within fast myocardial motion.

This work was supported in part by the European Research Council (ERC) through the European Union's Seventh Framework Programme (FP/2007–2013) under ERC Grant 311025 and in part by the Laboratory of Excellence ANR-10-LABX-24 (LABEX WIFI) within the French Program "Investments for the Future" under Grant ANR-10-IDEX-0001-02 PSL*. *(Corresponding author: Mathieu Pernot.)*

D. Maresca, M. Correia, M. Tanter, and M. Pernot are with CNRS UMR 7587, INSERM U979, Institut Langevin, ESPCI Paris, PSL Research University, 75012 Paris, France (e-mail: mathieu.pernot@espci.fr).

B. Ghaleh is with INSERM U955 Equipe 03, Ecole Nationale Vétérinaire d'Alfort, Université Paris-Est Créteil, 94000 Créteil, France.

Digital Object Identifier 10.1109/TUFFC.2018.2870083

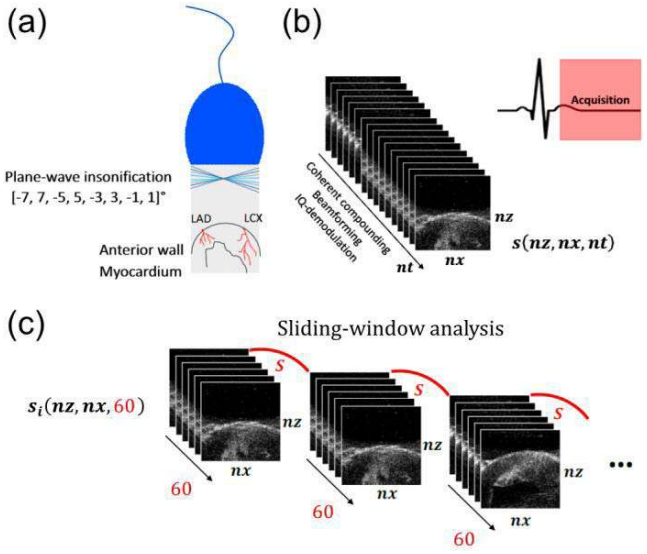

Fig. 1. (a) Ultrafast ultrasound insonification of the anterior myocardial wall, covering the LAD and left circumflex coronary territories. (b) Corresponding 0.3-s-long ultrafast ultrasound data set consisting in 1000 frames. (c) Decomposition of the original ensemble of frames into partially overlapping sliding ensembles of 60 frames before applying the power Doppler signal processing.

II. Material and Methods

A. Animal Handling

Two and a half months old (20–25 kg) female domestic swine (Sus scrofa domesticus) were anesthetized with isoflurane 2%, intubated, and ventilated. After sternotomy, the thorax was filled with saline at 37 °C for coupling of the ultrasound probe. The animal procedure was approved by the Institutional Animal Care and Use Committee of Ecole Veterinaire de Maison-Alfort (ComEth ANSES-ENVA-UPEC) according to the European Commission guiding principles (2010/63/EU).

B. Ultrasound Pulse Sequence and Data Preparation

We performed all image acquisitions with a linear 6-MHz ultrasound probe (Vermon, Tours, France) and a programmable ultrafast ultrasound scanner (Aixplorer, Supersonic Imaging, Aix-en-Provence, France). The ultrafast imaging sequence consisted in the transmission of eight tilted plane waves ($-7°$, $7°$, $-5°$, $5°$, $-3°$, $3°$, $-1°$, $1°$), leading to anterior myocardial wall imaging down to 4.5 cm and at a frame rate of 3280 images/s after coherent compounding [Fig. 1(a)] [7].

The 6-MHz center frequency of our probe (frequency used for pediatric cardiac applications) allowed for sampling of coronary blood flows below 42 cm/s. The full ultrafast Doppler acquisition lasted 305 ms (1000 frames), which covered the end-systolic and the full diastolic phases of the swine cardiac cycle under normal physiological conditions. The acquired data were beamformed using a conventional delay-and-sum algorithm and computed into complex and temporal in-phase

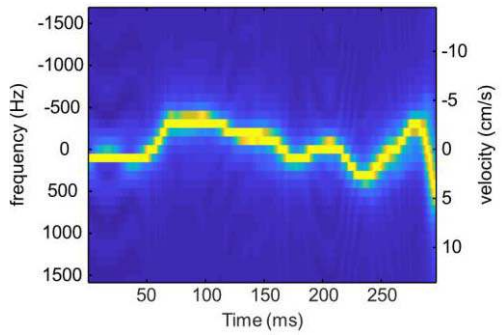

Fig. 2. Tissue Doppler frequency/velocity of the myocardial wall over the time of the ultrafast Doppler acquisition. The sliding window used was 8 ms long.

quadrature (IQ) signals. The resulting output was a 3-D matrix of size $nz \times nx \times nt$, where nz and nx are the number of pixels in the axial and lateral directions and nt is the number of frames acquired [Fig. 1(b)]. Coronary flow detection was performed on sliding ensembles of frames (typically ~50 frames or 15 ms), in which the cardiac tissue motion was considered to be small [Fig. 1(c)]. The overlap between frame ensembles was arbitrarily chosen to be 25% of the ensemble length (typically ~12 frames or 4 ms). In the rest of the text, we denote $s(x, z, t)$ as the raw IQ signal contained in each pixel of the frame ensemble.

C. Power Doppler Angiograms

Sliding IQ ensembles of frames were filtered to reject tissue clutter using a singular decomposition filter as reported by Demené *et al.* [8]. We denote $s_F(x, z, t)$ as the filtered signal containing blood and noise information after tissue signals rejection. Coronary angiograms were displayed by computing a power Doppler estimator, a metric proportional to blood flow and robust to aliasing [9]. The power Doppler intensity PwD was derived as follows:

$$\mathrm{PwD}(x, z) = \int_{i=1}^{N} |s_F(x, z, t)|^2 dt \tag{1}$$

where N is the ensemble number of frames. Directional power Doppler angiograms were derived by separating the positive and negative parts of the Doppler spectra [9].

D. Length of the Sliding Ensemble of Frames

On the one hand, the ensemble of frames should be taken as large as possible to increase the signal-to-noise ratio of Doppler estimates. On the other hand, the ensemble of frames should be taken small enough to ensure that tissue's scatterers stay on average in a focal zone during cardiac motion. We selected the sliding ensemble length by assuming that the mean axial displacement should not be larger than one wavelength within each sliding window through the entire acquisition, which corresponds to 257 μm at 6 MHz in biological tissue ($c = 1540$ m/s). We assessed the mean axial myocardial wall velocity using tissue Doppler imaging [10], as illustrated in Fig. 2, and found a mean absolute velocity over the entire acquisition of 1.35 cm/s. At this velocity, a 257-μm axial displacement takes 19 ms or 62 frames at our 3280-Hz framerate. Therefore, we arbitrarily selected a short ensemble length of 60 frames (or 18.3 ms) to stay just below that value. Note that this length was kept constant through diastole, but one could choose to adapt the sliding window length to cardiac motion.

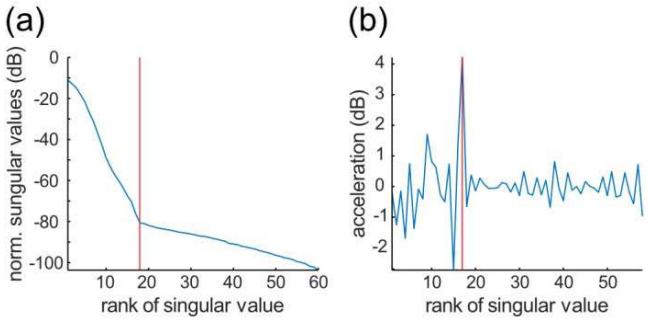

Fig. 3. (a) Normalized ordered singular values c_i in dB. (b) Acceleration $\ddot{c}_i$ of the normalized singular values. Red line: position of the maximum of $\ddot{c}_i$. The data represented here spanned from $t = 167$ to 185 ms.

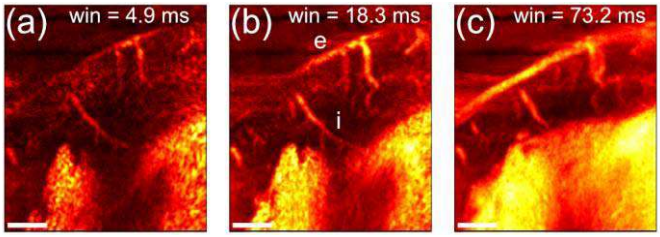

Fig. 4. Impact of window length on coronary Doppler angiography. (a) Power Doppler image of the myocardial coronary vasculature in diastole for a 4.9-ms-long, 16 frames window. (b) Same image for an 18.3-ms-long, 60 frames window; e indicates an epicardial vessel and i an intramural vessel. (c) Same image for a 73.2-ms-long, 240 frames window. The scalebars indicate 5 mm. For each window length, the first frame corresponds to $t = 167$ ms.

E. SVD Filter Adaptation Through the Cardiac Cycle

It was shown that singular value decomposition (SVD) filters are more efficient at separating blood signals from tissue clutter contained in ultrafast ultrasound data sets than conventional high-pass filters [8]. The beginning of our myocardial data set, which was triggered by the electrocardiogram, corresponded to the end-systolic phase of the cardiac cycle. During that phase that takes place right before the transition from venous to arterial coronary flow, the anterior wall of the myocardium remains relatively static for tenths of milliseconds. For the first 60 frames, we manually selected at an SVD cutoff value that provided a visually optimal image of the coronary vasculature. In the present data set, this initial cutoff value was set to 30 (50% of a total number of singular values). Next, for each sliding ensemble of frames, a new SVD was iteratively performed and the corresponding singular vectors and singular values were extracted. For each ensemble, we computed the metric c_i defined as the normalized ordered singular values

$$c_i = \lambda_i \Big/ \sum_i \lambda_i, \quad \text{with} \sum_{i=1}^{60} c_i = 1 \tag{2}$$

where λ_i are the singular values of the SVD. c_i measures the relative weight or percentage of information of the original data contained in each singular value [Fig. 3(a)] [11]. Finally, for each ensemble of 60 frames, we computed $\ddot{c}_i$, the second derivative (or acceleration) of the normalized singular values converted to decibel [Fig. 3(b)]. The maximum of $\ddot{c}_i$ localizes the main inflection point of c_i. In practice, that point separates

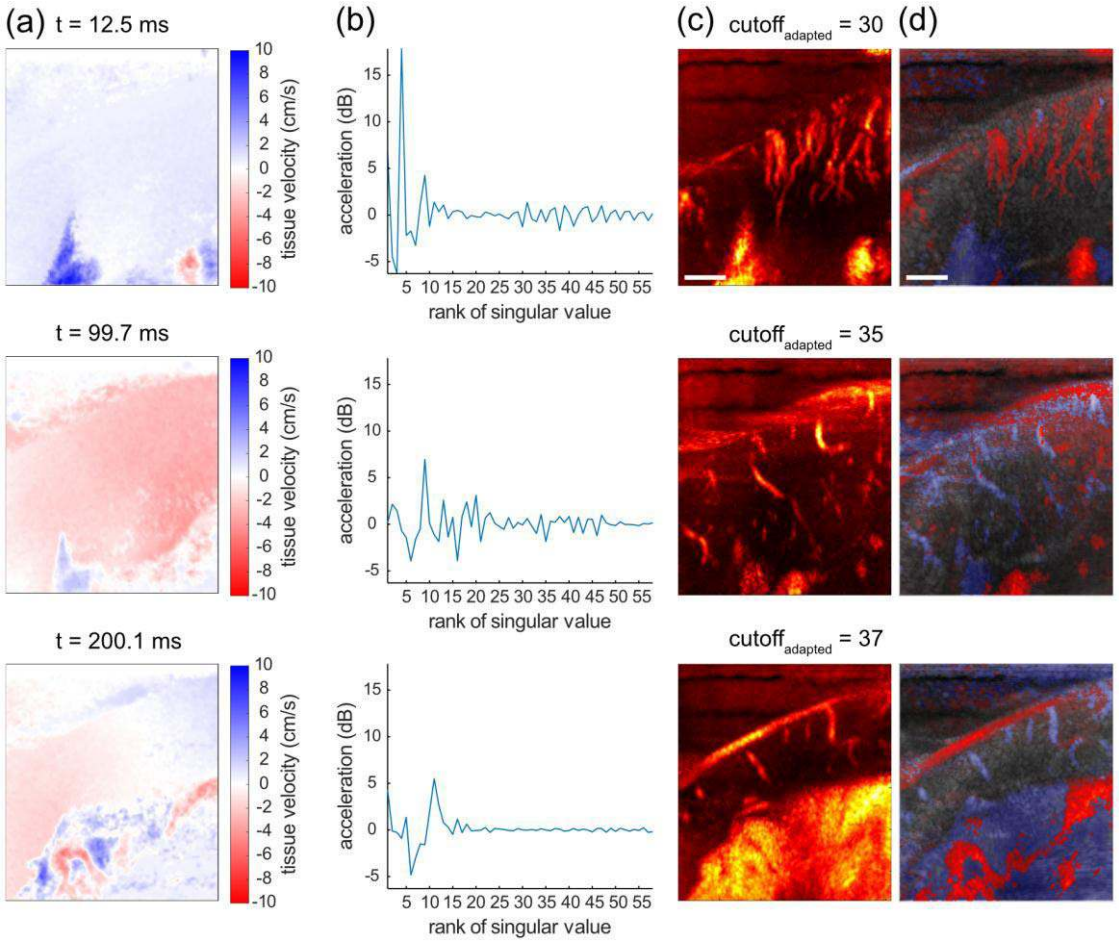

Fig. 5. Adaptation of the SVD filter from end-systole to end-diastole. The parameter k was fixed to 26. (a) Tissue Doppler imaging of the anterial wall at three different times of the swine cardiac cycle. (b) Second derivative of the normalized singular values at three different times of the swine cardiac. (c) Power Doppler images of the coronary vasculature after SVD filtering with cutoff adaptation. (d) Adapted directional power Doppler overlaid on anatomical ultrasound images of the anterior wall at three different times of the swine cardiac. The scalebars represent 5 mm.

coherent information such as tissue signals, which is contained in the first singular values and exhibits rapidly decaying singular values, from incoherent information (blood and noise) which is contained in the rest of the singular values and exhibits a slower slope [Fig. 3(a)].

For each ensemble of frames, we tracked the position of the maximum of $\ddot{c}_i$ and used that position index to adapt the SVD cutoff value. The adaptation of the SVD filter cutoff, which separates blood signals from the tissue clutter through diastole, was performed in each frame ensemble as follows:

$$s_F(x,z,t) = s(x,z,t) - \sum_{i=1}^{\arg\_\max(\ddot{c}_j)+k} \lambda_i U_i(x,z) V_i(t) \qquad (3)$$

where $1 < j < N$ where N is the number of eigenvectors, U and V are the spatial and temporal singular vectors of $s(x,z,t)$ [8] and k is a constant that can be arbitrarily chosen by the operator to adjust the initial cutoff result at the beginning of the diastolic phase.

III. Results

CUDA was successful in imaging the epicardial and intramural coronary vasculature in spite of the myocardial wall motion (up to 5 cm/s in this acquisition as shown in Fig. 2). Fig. 4 displays the impact of the ensemble length on the power Doppler images of the coronary vasculature. All SVD cutoffs were set to 50% of the ensemble length (8, 30, and 120, respectively). With a 16 frames ensemble (4.9 ms), the coronary vasculature was barely visible and vessels were missing [Fig. 4(a)]. With a 60 frames ensemble (18.3 ms), the epicardial vessels appeared and the resolution and contrast were enhanced [Fig. 4(b)]. With a 240 frames ensemble (73.2 ms), the angiogram was blurred due to myocardial wall motion [Fig. 4(c)]. This result validates the choice of a 60 frames window length.

Results reported in Fig. 5 show the adaption of the SVD filter cutoff in end-systole and diastole using the second derivative of the normalized singular values. Tracking the maximal acceleration of the normalized singular values led to high contrast images of the coronary vasculature with reduced clutter, revealing both coronary veins [Fig. 5(c) and (d), top row] and arteries [Fig. 5(c) and (d), middle and bottom rows]. Directional power Doppler angiograms successfully captured the inversion of blow taking place between systole and diastole [Fig. 5(d)]. In systole, blood was flowing up to the epicardium and down along epicardial vessels, while in diastole, it flowed up along the epicardial vessels and down toward the endocardium.

IV. Conclusion

In this letter, we investigated the performance of an adaptive spatiotemporal filter for CUDA [6]. To the best of our knowledge, CUDA is the first medical imaging technology with

enough sensitivity and resolution to visualize the intramural coronary vasculature in a beating heart. In the present example, CUDA had a temporal resolution of 18.3 ms and a spatial resolution of the order of 100 μm and successfully revealed the coronary vasculature from end-systole to end-diastole in an open-chest swine experiment. Our processing method is successfully adapted to cardiac motion through the evaluation of the information contained in the normalized singular values of IQ data, paving the way toward a fully automated coronary flow imaging modality. Note that the processing reported here was not a real-time implementation, but commercial ultrafast ultrasound scanners are capable of processing live Doppler angiograms.

The present study was limited to the anterior wall of the myocardium, which is the territory of the left anterior descending (LAD) artery, one of the two major coronary arteries. However, deeper segments of the heart were not imaged. This will necessitate the use of lower frequencies than the pediatric cardiac frequency selected here. The sensitivity of the CUDA method to arterioles at 3 MHz or below has not been investigated.

On the processing front, one could attempt to vary the ensemble length through the heart cycle as a function of cardiac motion; this approach was not evaluated here. In addition, the signal-to-noise ratio could be improved further by relying on coded excitation transmission matrices [12]. This strategy could help imaging deeper vessels or resolving smaller ones at our current examination depth (<4.5 cm). Another limitation of the method is the arbitrary k value which could differ in human applications.

Our tissue motion processing was also limited to the axial component estimation. In the future, full myocardial wall motion including lateral component could be characterized and corrected over short ensemble lengths using vector Doppler or Speckle tracking algorithms.

Even though the appeal of CUDA is to be a potentially fully noninvasive technique, the use of ultrasound contrast agents is another avenue to enhance signal-to-noise ratio further in ultrafast echocardiography [13]. The potential of myocardial contrast echocardiography has been extensively discussed [14], even though its adoption remains limited.

In the future, CUDA may be used in clinical practice to characterize noninvasively the coronary function by the quantitative assessment of the coronary flow reserve [6].

REFERENCES

[1] P. G. Camici, G. D'Amati, and O. Rimoldi, "Coronary microvascular dysfunction: Mechanisms and functional assessment," *Nature Rev. Cardiol.*, vol. 12, pp. 48–62, Oct. 2015.

[2] S. D. Fihn *et al.*, "2014 ACC/AHA/AATS/PCNA/SCAI/STS focused update of the guideline for the diagnosis and management of patients with stable ischemic heart disease: A report of the american college of cardiology/american heart association task force on practice guidelines, and the american association for thoracic surgery, preventive cardiovascular nurses association, society for cardiovascular angiography and interventions, and society of thoracic surgeons," *J. Thoracic Cardiovascular Surg.*, vol. 149, pp. e5–e23, Mar. 2015.

[3] M. Cikes, L. Tong, G. R. Sutherland, and J. D'Hooge, "Ultrafast cardiac ultrasound imaging: Technical principles, applications, and clinical benefits," *JACC, Cardiovascular Imag.*, vol. 7, no. 8, pp. 812–823, Aug. 2014.

[4] B. F. Osmanski, M. Pernot, G. Montaldo, A. Bel, E. Messas, and M. Tanter, "Ultrafast Doppler imaging of blood flow dynamics in the myocardium," *IEEE Trans. Med. Imag.*, vol. 31, no. 8, pp. 1661–1668, Aug. 2012.

[5] B.-F. Osmanski, D. Maresca, E. Messas, M. Tanter, and M. Pernot, "Transthoracic ultrafast Doppler imaging of human left ventricular hemodynamic function," *IEEE Trans. Ultrason., Ferroelectr., Freq. Control*, vol. 61, no. 8, pp. 1268–1275, Aug. 2014.

[6] D. Maresca *et al.*, "Noninvasive imaging of the coronary vasculature using ultrafast ultrasound," *JACC, Cardiovascular Imag.*, vol. 11, no. 6, pp. 798–808, Jun. 2017.

[7] G. Montaldo, M. Tanter, J. Bercoff, N. Benech, and M. Fink, "Coherent plane-wave compounding for very high frame rate ultrasonography and transient elastography," *IEEE Trans. Ultrason., Ferroelectr., Freq. Control*, vol. 56, no. 3, pp. 489–506, Mar. 2009.

[8] C. Demené *et al.*, "Spatiotemporal clutter filtering of ultrafast ultrasound data highly increases Doppler and ultrasound sensitivity," *IEEE Trans. Med. Imag.*, vol. 34, no. 11, pp. 2271–2285, Nov. 2015.

[9] E. Mace, G. Montaldo, B. Osmanski, I. Cohen, M. Fink, and M. Tanter, "Functional ultrasound imaging of the brain: Theory and basic principles," *IEEE Trans. Ultrason., Ferroelectr., Freq. Control*, vol. 60, no. 3, pp. 492–506, Mar. 2013.

[10] C. Kasai, K. Namekawa, A. Koyano, and R. Omoto, "Real-time two-dimensional blood flow imaging using an autocorrelation technique," *IEEE Trans. Sonics Ultrason.*, vol. SU-32, no. 3, pp. 458–464, May 1985.

[11] C. Bécavin, N. Tchitchek, C. Mintsa-Eya, A. Lesne, and A. Benecke, "Improving the efficiency of multidimensional scaling in the analysis of high-dimensional data using singular value decomposition," *Bioinformatics*, vol. 27, no. 10, pp. 1413–1421, May 2011.

[12] E. Tiran *et al.*, "Multiplane wave imaging increases signal-to-noise ratio in ultrafast ultrasound imaging," *Phys. Med. Biol.*, vol. 60, no. 21, pp. 8549–8566, Nov. 2015.

[13] M. E. G. Toulemonde *et al.*, "High frame-rate contrast echocardiography: In-human demonstration," *JACC, Cardiovascular Imag.*, vol. 11, no. 6, pp. 923–924, Dec. 2017.

[14] T. R. Porter and F. Xie, "Myocardial perfusion imaging with contrast ultrasound," *JACC, Cardiovascular Imag.*, vol. 3, pp. 176–187, Feb. 2010.